OPEN ACCESS

Article

Nano Biomed Eng

ISSN 2150-5578 http://nanobe.org

# Synthesis, Optical and Photocatalytic Properties of ZnSe Microspheres/Nanosheets

Yongqiang Yang, Yan Zhang, Xuejiao Zhou, Xiaochen Wu, Sizhe Xu, Haixia Wu*, and Shouwu Guo*

National Key Laboratory of Micro/Nano Fabrication Technology, Key Laboratory for Thin Film and Microfabrication of the Ministry of Education, Research Institute of Micro/Nano Science and Technology, Shanghai Jiao Tong University, Shanghai 200240, China

* Corresponding author: swguo@sjtu.edu.cn (Shouwu Guo) and haixiawu@sjtu.edu.cn (Haixia Wu)

## Abstract

The microspheres/nanosheets of the ZnSe were prepared by solvothermal route. The morphological, structural, optical, as well as photocatalytic properties of the ZnSe products were studied. SEM and TEM results showed that morphologies of the products were sensitive to the presence of water or not, and a mechanism was proposed. The products shows a weak blue emission band centered at 476 nm, which is attributed to the near-band-edge emission of the products, and the strong and broad peak at 520 nm is attributed to a defect-related emission. The PL and XRD results indicate that ZnSe microspheres have high crystalline and few defects compared with ZnSe nanosheets, the degradation for Rhodamine 6G shows that the photoactivity of ZnSe nanosheets is nearly twice that of ZnSe microspheres. Therefore, the decrease of defects implies the decrease of photocatalytic activity, and nanosheets is more suitable for the degradation of Rhodamine 6G.

**Keywords:** ZnSe, Microspheres, Nanosheets, Photoluminescence, Photocatalytic

**Citation**: Y. Yang, et al. Synthesis, Optical and Photocatalytic Properties of ZnSe Microspheres/Nanosheets. Nano Biomed. Eng. 2011, 3(2), 107-114. DOI: 10.5101/nbe.v3i2.p107-114.

## 1. Introduction

Zinc selenide (ZnSe), as one of the important Zn-based Ⅱ - Ⅵ semiconductors, due to its wide direct band gap (2.67 eV) and large excition binding energy (21 meV) [1, 3], has been considered to be a promising material for optoelectronic devices, including blue laser diodes, light-emitting diodes, photodetectors and photosensitivity [4, 6]. Moreover, ZnSe has been employed as labeling tags in bioassays due to its high biocompatibility [7, 10]. Therefore, ZnSe is of great interest as a model material in such forms as thin films, quantum wells quantum dots, bulk crystals, and ZnSe-based optoelectronic devices [11, 12].

In recent years, Ⅱ - Ⅵ semiconductor wires [13], belts [14], rods [15], tube [16], plates [17], core/shell18, spheres [19-21], and complicated hierarchical structures [22] have been successfully synthesized by several methods. Among these structures, spherical shape and sheets structures have attracted tremendous attentions due to their high packing densities and high specific surface. For example, Wang et al. [20] synthesized ZnSe microspheres by hydrothermal reaction of $ZnSO_4$•$7H_2O$ and $NaSeSO_3$ with the assistance of surface-active polyethylene glycol. Du et al. [17] synthesized ZnSe nanoflakes by solvothermal reaction of $ZnCl_2$ and Se in a mixed solvent of ethylenediamine and hydrazine hydrate. And Yao et al. [21] synthesized an inorganic-organic hybrid semiconductor nanobelt $[ZnSe](DETA)_{0.5}$ (DETA=diethylenetriamine) in ternary solution. Although attempts have been tried, little work has been done to realize the transformation between sphere and sheet only through the adjusting of the ratio of water and additives.

In this article, we reported the synthesis of ZnSe microspheres and nanosheets under mild solvothermal conditions. And their optical and photocatalytic properties of the two structures of the ZnSe products were studied.

## 2. Experimental Section

### 2.1 Preparation of ZnSe microspheres and nanosheets

All chemicals used in this experiment were of analytical grade and were used without further purification.

### 2.1.1 Microspheres

In a typical synthesis procedure, $ZnCl_2$ (0.218 g, 1.6 mmol), elemental Se power (0.118 g, 1.5 mmol), the mass ratio of NaOH to $ZnCl_2$ is 4.6: 1 and $H_2O$ (20 ml) were added into 20 mL mixed solution with a ratio between absolute ethanol and oleic acid of 3:1. The solution was then transferred into an 80 mL sealed Teflon autoclave, and the reaction temperature was rapidly increased up to 180 °C. The solution was kept at this temperature for 24 h, and after the heating treatment, the autoclave was cooled to room temperature naturally. The products were collected by centrifugation, washed three times with deionized water and absolute ethanol, respectively, and then dried at 50 °C; as a result, yellow powders were obtained.

### 2.1.2 Nanosheets

Exception eliminating water, keeping the conditions do not changes. At last, reddish brown powers were obtained.

### 2.2 Characterization

The phases of samples were identified by X-ray diffraction (XRD) patterns obtained on a Philips X'Pert Pro Super diffractometer with graphite-monochromatized Cu Kr radiation (λ=1.54178 Å). The morphologies and microstructures of samples were examined by scanning electron microscopy (SEM) (Hitachi F-4800), transmission electron microscopy (TEM) (JEOL JEM-2100F). Room-temperature Raman spectra were measured using a microlaser Raman spectrometer (Renishaw) in a backscattering configuration, employing the 514.5 nm line of Ar laser as the excitation source. The IR spectrum was recorded using a Nicolet NEXUS670 transform IR spectrophotometer at room temperature with the samples milled in KBr wafer. Photoluminescence (PL) spectra were measured on an ENDINBURGH FLS 920 spectrophotometer at the excitation wavelength of 325 nm.

### 2.3 The photocatalytic activity test of ZnSe microspheres/nanosheets

The photocatalytic activity test of ZnSe microspheres/nanosheets were investigated by evaluating in terms of the degradation of Rhodamine 6G (Rh-6G)solution under UV irradiation. A 300 W high-pressure mercury lamp with main emission wavelength 365 nm (Shanghai Bilon Instruments Co. Ltd), was set inside a cylindrical reactor, and surrounded by a circulating water jacket to cool the lamp and minimize infrared radiation. 50 mg of ZnSe products were suspended in 100 ml of an aqueous solution of $10^{-5}$ M Rh-6G. The solutions were continuously stirred for about 30 min at room temperature to ensure the establishment of an adsorption-desorption equilibrium among the photocatalyst, Rh-6G, and water, before irradiation with light from the high-pressure mercury lamp. The distance between the light source and the solution was about 10 cm. The concentrations of Rh-6G were monitored by using a UV-vis spectrometer (Shimadzu, Japan. UV-2500).

## 3. Results and Discussion

The morphology and structure of the as-prepared ZnSe were studied using SEM, and XRD. Fig. 1(a)-(c) show typical SEM images of the spherical structures with the diameters of about 4 μm, which are composed of sub-particles in the range of 100-300 nm as shown in Fig. 1c. The XRD pattern of the as-prepared sample (Fig. 1d) reveals that the products are cubic ZnSe phases (JCPDS Card, No. 70-0777) with the lattice constants of

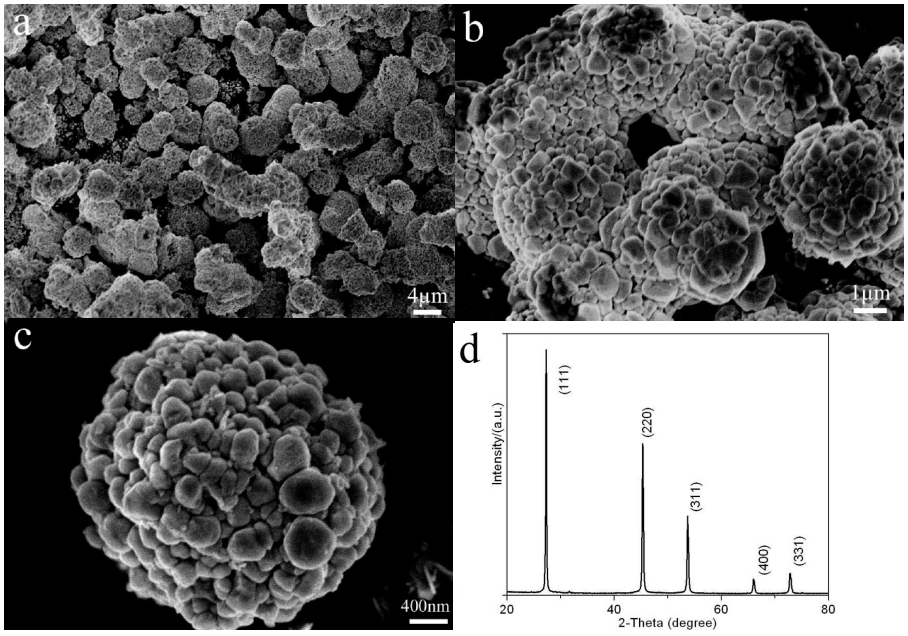


**Fig. 1** TEM (a) and HRTEM (b) image of the as-prepared ZnSe particles. The inset of Fig.2b shows a two-dimensional Fourier transform pattern of the lattice resolved image.

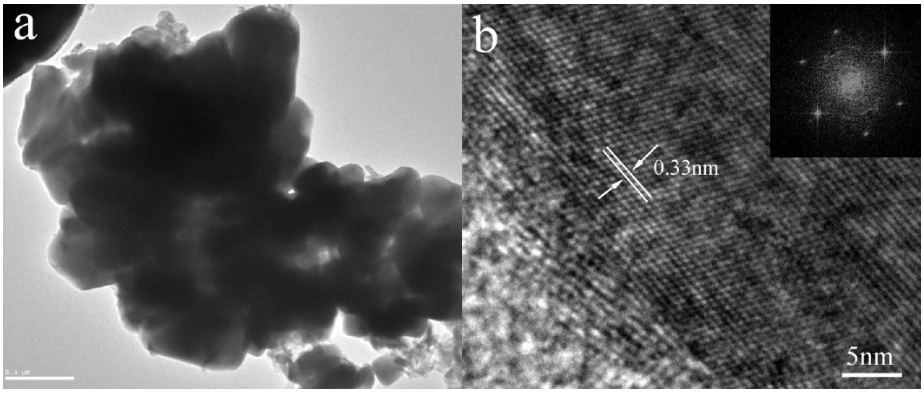


**Fig. 2** TEM (a) and HRTEM (b) image of the as-prepared ZnSe particles. The inset of Fig.2b shows a two-dimensional Fourier transform pattern of the lattice resolved image.

a= 5.633 Å. No peaks of any other phase were detected, which indicates that the as-prepared sample is pure ZnSe with a zinc blende structure.

The structure and morphology of the products were further observed by high-resolution TEM (HRTEM). Fig. 2a shows a typical TEM image of ZnSe particles, which resulted from the ultrasonic decomposition of ZnSe microspheres during the sample preparation for TEM observation. It shows that a large amount of irregular particles, which are in the range of 100-300 nm diameters, are randomly distributed onto the copper mesh. Fig. 2b shows a HRTEM image and a two-dimensional Fourier transform pattern (the inset of Fig. 2b). The HRTEM image indicates a clear lattice spacing of 0.33 nm which corresponds to the interplanar distance of (111) lattice planes of cubic ZnSe phases, and its two-dimensional FFT pattern further demonstrates the single crystalline structure of ZnSe particles.

The effect of the deionized water (DIW) on the morphology of products has been reported in the literature [22]. So a control experiment that without the addition of DIW was done here, and the SEM images of the products are exhibited in Fig. 3a. It shows that the morphology of products is nanosheets but not microspheres, and the thickness of the nanosheet is about 90 nm (the inset of Fig. 3a). The Fig. 3b shows the XRD pattern of the products, and it reveals that the products are also pure-phase cubic ZnSe. Compared with the diffraction spectra of ZnSe microspheres (as shown in Fig. 1d), the peaks of ZnSe sheets are broader, which indicates the increase of the ZnSe nanocrystallites, and the sheet structure was further confirmed as shown in Fig. 3c. It shows that the nanosheet is crystallized with clear lattice fringes parallel to the wall from the high-resolution TEM image (Fig. 3d). The inter-plane distance of 0.33 nm agrees well with the separation between the (111)

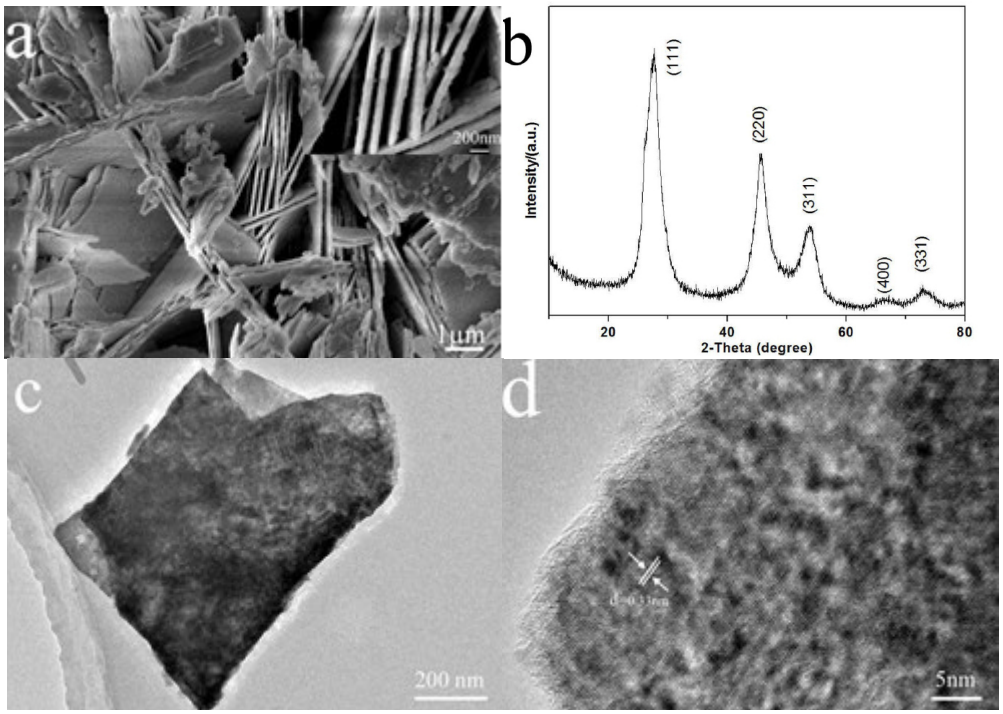


**Fig. 3** In the case of without water, the SEM images (a) and XRD pattern (b) of products. Inset is the magnification image; TEM (c) and HRTEM (d) images

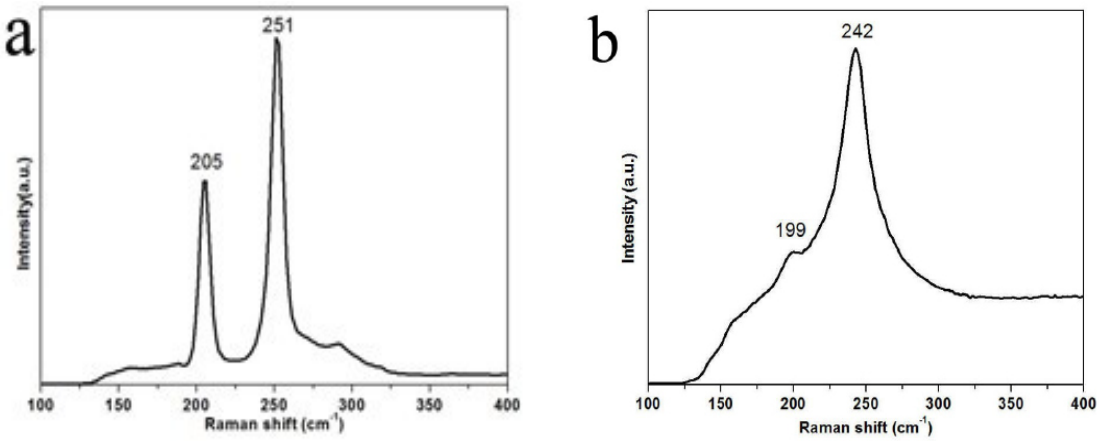


**Fig. 4** The typical room-temperature Raman spectrum of the as-prepared ZnSe microspheres (a) and ZnSe nanosheets(b).

lattice planes.

The as-synthesized products were further examinedby Raman and PL spectroscopy. Raman scattering spectroscopy was employed to study the structures of the ZnSe structures. It is well known that the TO and LO phonon frequencies for bulk ZnSe are 210 and 255 $cm^{-1}$ [23, 24]. Fig. 4a shows a typical room-temperature Raman spectrum of the ZnSe microspheres. Two Raman peaks centered at 205 and 251 $cm^{-1}$ are observed, which are attributed to the transverse optic (TO) and longitudinal optic (LO) phonon modes of crystal ZnSe, respectively. The sharp and symmetrical Raman peaks disclose that the ZnSe structures are all of high crystalline quality and pure phase [12, 22, 25], which are consistent with the above SEM and XRD results. For the ZnSe nanosheets, however, the TO and LO phonon frequencies centered at 199 and 242 $cm^{-1}$, respectively, and both give a broad Raman peak due to the high surface-to-volume ratio of the structures [12, 22]. Compared to the Raman peaks of the bulk ZnSe [23, 24], that of the ZnSe microspheres and nanosheets both are shifted toward lower frequency, which is probably due to the effect of special fine or nanostructures [12, 22, 25].

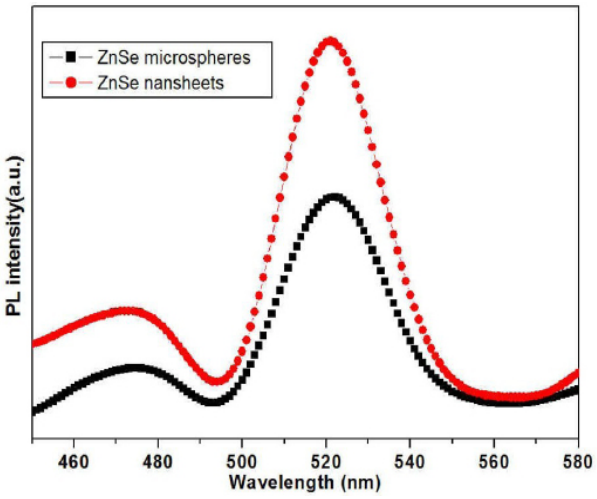


**Fig. 5** PL spectra of the ZnSe microspheres and nanosheets

The room-temperature PL spectra of ZnSe microspheres and nanosheets both show a weak blue emission band centered at 476 nm, and a strong and broad emission band ranging from 500 to 540 nm(Fig. 5). The weak blue emission peak is usually attributed to the near-band-edge (NBE) emission of ZnSe [2, 26]. While the emission band from 500 to 540 nm has been associated with the surface emissions and possible metal vacancies [27, 30]. Geng et al. [19] explained the strong emission around 520 nm as a result of some donor-acceptor pairs that are related to Zn vacancy and interstitial states, or associated with dislocations stacking faults, and nonstoichiometric defects. Zhang et al. [21] explained the emission was attributed to recombination of a donor-acceptor pair involving Zn vacancies and Zn interstitial. Because of the products growth at Zn-rich condition, so we believe that the strong emission must be attributed to the interstitial Zn defect and nonstoichiometric defects.

In order to investigate the photocatalytic activity of the ZnSe microspheres and nanosheets, Rh-6G($10^{-5}$ M) was chosen as the photocatalytic degradation dye. The characteristic absorption of Rh-6G at λ=524 nm is selected as monitoring the photocatalytic degradation process. The target molecule Rh-6G is relatively stable in aqueous solution when it is exposed to visible light irradiation. The control analyses show that the degradation of Rh-6G is negligible in the absence of ZnSe catalysts. The degradations of the Rh-6G in the presence of ZnSe microspheres (Fig. 6a) and ZnSe nanosheets (Fig. 6b) were measured with a 300 W high-pressure mercury lamp irradiation ($\lambda_{max}$=365 nm) at 283 K at various times. The resulted indicates that the ZnSe nanosheets show higher photoactivity and 44% of the Rh-6G dye was degraded after 120 min (Fig. 6c). This is attributed to the larger surface-to-volume ratio of ZnSe nanosheets than that of

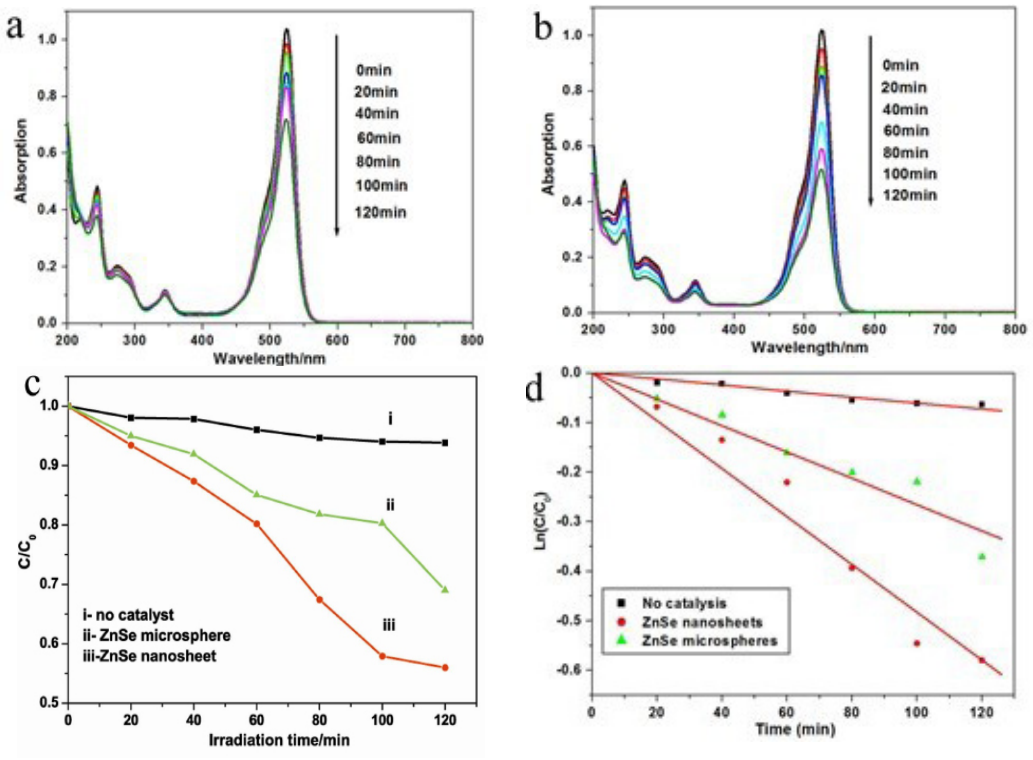


**Fig. 6** UV-visible absorption spectral changes for Rh-6G solutions in the presence of (a) ZnSe microspheres, and (b) ZnSe nanosheets. (c) Photodegradation curves of Rh-6G in water under UV light in the presence of catalysts (ZnSe microspheres and ZnSe nanosheets), without adding any catalyst. (d) The selected fitting results using the pseudo-first-order reaction.

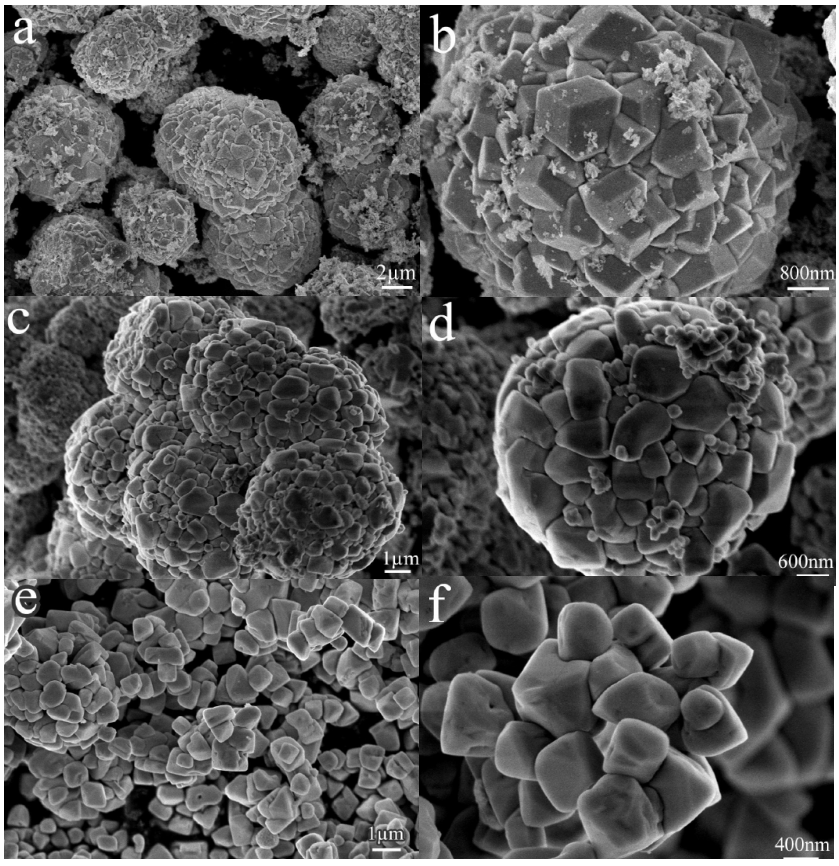


**Fig. 7** The morphologies of products with different reaction conditions (a) 150 °C, 24 h; (b) 180 °C, 48 h; (c) 180°C, 24 h, the mass ratio is 14:1 between NaOH and $ZnCl_2$.

microspheres, which helps to increase the photocatalytic reactions sites and promote the electron-hole separation. Under UV light irradiation, the pseudo-first-order constants for the photodegration of Rh-6G are 0.00266 $min^{-1}$ and 0.00483 $min^{-1}$ with ZnSe microspheres or ZnSe nansheets, respectively (Fig. 6d). The linear relationship between $\ln c/c_0$ and time $t$ can be achieved for both of the two selected photodegradation curves of ZnSe microspheres and ZnSe nanosheets. And the degradation rate of ZnSe nanosheets is nearly twice that of ZnSe microspheres. Additionally, the PL and XRD results indicate that ZnSe microspheres have high crystalline and few defects compared with ZnSe nanosheets. Defects may serve as recombination centers for photoexcited electron-hole pairs during photocatalysis, therefore, the decrease of defects implied the decrease of photocatalytic activity.

To disclose the morphology evolution of the ZnSe microspheres, a series of control experiments were performed. The effects of several parameters (such as temperature, reaction time, and pH value) on the formation of ZnSe microspheres structures were studied. Fig. 7(a-b) are the SEM images of the products obtained at 150 °C for 24 h, compared with the microspheres gained at 180 °C, 24 h (as shown in Fig. 1), which clearly shows that the obtained products are larger microspheres with a diameter of about 4-10 μm, and the sub-particles of the microspheres are in the range of 0.8-1.5 μm. When the products obtained at 180 °C and the reaction time is prolonged for 48 h, compared with 24 h (as shown in Fig. 1), it can found that the diameter of these microspheres and the sub-particles are also increased, and the diameter are in range of 5-6 μm and 300-700 nm, respectively (Fig. 7c-d). In addition, with the mass ratio (NaOH to $ZnCl_2$) increased to 14:1, we can found that the microspheres is difficulty to form (Fig. 7(e-f )).

At the same time, the morphology of ZnSe nanosheets was also changed at different reaction condition. When the reaction temperature was at 150 °C for 24 h, besides ZnSe sheets, a certain amount of spherical products were observed (Fig. 8a,b). In the case of increasing reaction time, the morphology of products do not change, but the thickness of sheets is slightly increased (Fig. 8c,d). However, the impact of the base amount is notable, the thickness of the products increased from 90 nm to about 400 nm when the mass ratio of NaOH and $ZnCl_2$ changed from 4.6 to 14(Fig. 8e,f).

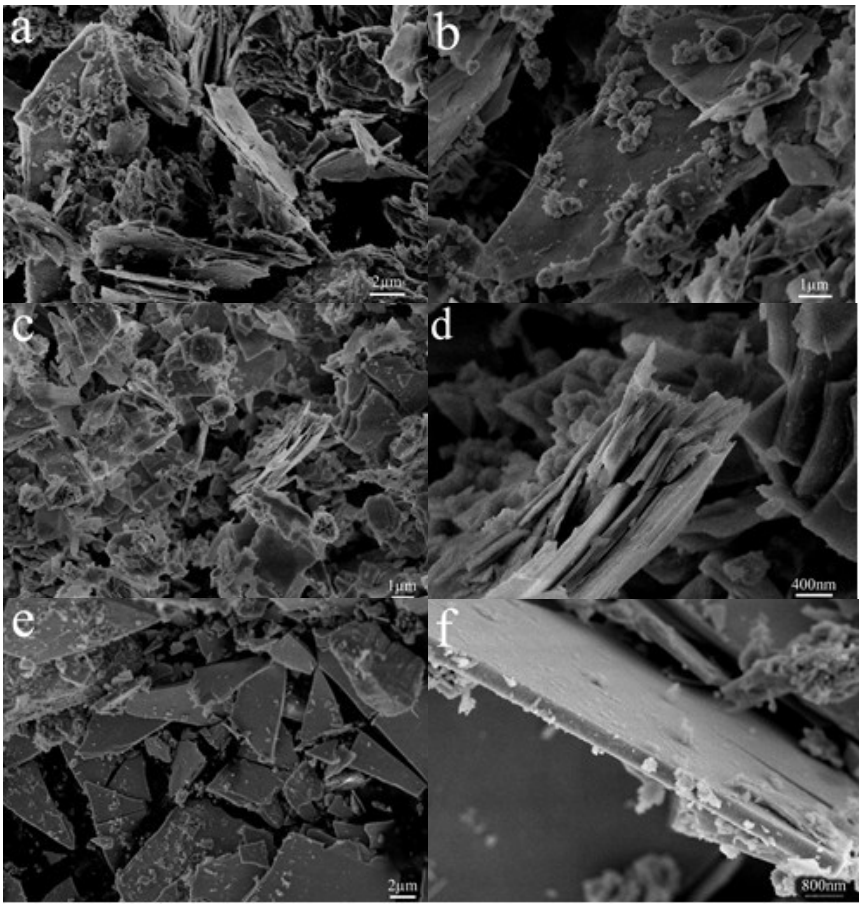


**Fig. 8** The morphologies of products with different reaction conditions (a) 150 °C, 24 h; (b) 180 °C, 48 h; (c) 180°C, 24 h, NaOH: $ZnCl_2$ is 14:1(mass ratio)

The above results indicate that the morphology and size of the products could be controlled by the reaction parameters (such as temperature, reaction time, and pH value). However, except the deionized water, other parameters did not show great striking impact on the morphology of the products, which indicates that the water plays a key role in the formation of different shaped products.

To investigate the effect of oleic acid, an IR measurement was carried out to reveal the function of the oleic molecules (Fig. 9). The sharp peak at 1380 $cm^{-1}$ seen in the spectrum is an artifact due to the IR instrument. The peak was regularly (though not always) observed even in spectra recorded with pure KBr [31]. The broad band at ~3400 and 1630 $cm^{-1}$ in the spectrum can be partly attributed to the $v$ (O-H) stretch of absorbed water on the sample. For pure oleic acid, the $v$ (O=H) stretch appears at 1711 $cm^{-1}$, and this peak is absent in the infrared spectrum of ZnSe coated with oleic acid in Fig. 9. Instead, a characteristic band appears at 1464 $cm^{-1}$, corresponding to the symmetric, $v_s(COO^-)$ stretch. The peaks at 2925 $cm^{-1}$ is assigned to the antisymmetric methylene stretches ($v_{as}(CH_2)$) of the oleic acid molecule. The antisymmetric methyl stretch, $v_{as}$ ($CH_3$), is seen as a shoulder on the peak at 2970 $cm^{-1}$ [31, 32]. This result leads to the conclusion that the oleic acid molecules adsorbed on the ZnSe nanocrystals all have the hydrophobic alkyl group directed away from the surface.

On the basis of the above facts, we have a primary understanding of the growth and self-assembly process of ZnSe products as followed (as shows Fig. 10): Our synthesis procedure involves the precipitation of the zinc salts and selenium ions in the presence of excess oleic acid molecules. When the mixture of oleic acid and ethanol was added, part of the oleic acid was converted into sodium oleate, forming a two-phase water/oil system. Oleic acid is excess in the system, so the zinc ion will form complexes easily with one to two oleic acid molecules and will be stabilized by the excess oleic acid. The function of oleic acid in the current method may base on the selective-adsorption model, which is similar to that of the alkyl chain phosphonic acids, in which the mixed solvents are selectively adsorbed at different crystallographic facets of the growing crystals to achieve anisotropic crystal growth kinetically [33]. During the reaction process, along with the Se powder reacted with NaOH to form $Se^{2-}$, the OA-capped Zn ions have a great chance of reacting with $Se^{2-}$ to form ZnSe nuclei at the interface of water and oleic acid, because the diffusion rate of molecules/ions was sped up at the elevated temperature. After the initial nucleation, the ZnSe monomers will grow into ZnSe crystallites, driven by the minimization of the total energy of the system, these ZnSe crystallites will aggregate together to form solid microspheres. In addition, the use of oleic acid with ethanol may also lead to some fluctuations at 150-180 °C in the present system, which can lead to the formation of the ZnSe microspheres with irregular fine particles. When the DIW was excluded in the reaction solution, however, the viscosity is also increased, because of oleic acid is a long alkyl chain carboxylic acid with high viscosity, so the diffusion process of the ZnSe nanocrystals cannot be well conducted in such highly viscous that the final sheets were obtained.

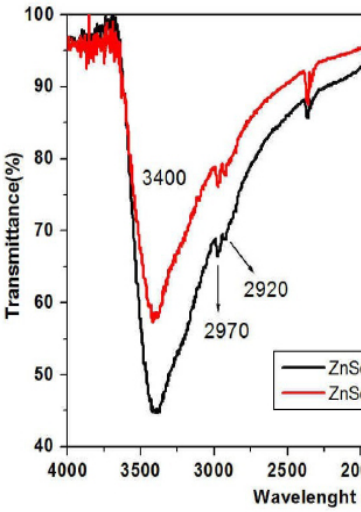


**Fig. 9** Fourier transform IR spectrum of ZnSe microspheres and ZnSe nanosheets.

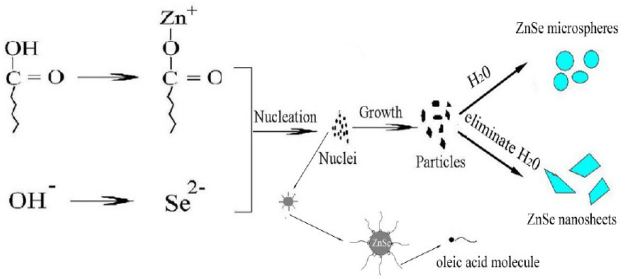


**Fig. 10** A schematic illustration of the process for the formation of ZnSe microspheres and ZnSe nanosheets.

## 4. Conclusion

In summary, the microspheres and nanosheets of ZnSe with a cubic structure have been successfully synthesized via solvothermal routine. The diameters of the microspheres about 4 μm, which are composed of sub-particles, and diameter of the sub-particles are in the range of 100-300 nm, while the thicknesses of the nanosheets is about 90 nm. The PL of the products shows a strong emission band at about 520 nm which attributed to the interstitial Zn defect and nonstoichiometric defects, and a weak NBE emission band at 476 nm. According to the degradation of Rh-6G, the degradation rate of ZnSe nanosheets is nearly twice that of ZnSe microspheres, which suggests that the as-synthesized ZnSe nanosheets are a more powerful photocatalyst for the degradation of Rh-6G dye. Through changing the morphologies and the IR spectra revealed that the deionized water and the oleic acid molecules play an important role in the growth of ZnSe microspheres and nanosheets.

## Acknowledgements

This work was financially supported by the National "973" Program (Nos. 2007CB936000 and 2010CB933900) and the NSFC (No. 20774029 and No. 20906055) of China and China postdoctoral science foundation (No. 20100470131).

## References

1. Malik MA, Revaprasadu N, O'Brien P. Air-stable single source precursors for the synthesis of chalcogenide semiconductor nanoparticles. *Chem. Mater.* 2001; 13: 913-920. doi: 10.1021/Cm0011662
2. Xiong SL, Shen JM , Xie Q, Gao YQ, Tang Q, Qian YT. A precursor-based route to ZnSe nanowire bundles. *Adv. Funct. Mater.* 2005; 15: 1787-1792. doi:10.1002/adfm.200500069
3. Wang CR, Wang J, Li Q, Yi GC. ZnSe-Si bi-coaxial nanowire heterostructures.*Adv. Funct. Mater.* 2005; 15:1471-1477. doi: 10.1002/adfm.200400564
4. Zhang LH, Yang HQ, Yu J, Shao FH, Li L, Zhang FH, Zhao H. Controlled synthesis and shotocatalytic activity of ZnSe nanostructured assemblies with different morphologies and crystalline phases. *J. Phys. Chem. C.* 2009; 113:5434-5443.doi:10.1021/Jp810385v
5. Tafreshi MJ, Balakrishnan K, Dhanasekaran R. Micromorphological studies on the ZnSe single crystals grown by chemical vapour transport technique. *J. Mater. Sci.* 1997; 32: 3517-3521.
6. Kouklin N, Menon L, Wong AZ, Thompson DW, Woollam JA, Williams PF. Bandyopadhyay S. Giant photoresistivity and optically controlled switching in self-assembled nanowires. *Appl. Phys. Lett.* 2001; 79: 4423-4425. doi:10.1063/1.1427156
7. Li L, Zhang FF, Ding YP, Wang Y P, Zhang LL. Synthesis of functionalized ZnSe nanoparticles and their applications in the determination of determination of bovine serum albumin. *J FLUORESC* 2009; 19: 437-441. doi: 10.1007/s10895-008-0430-2
8 . Yao JJ, Schachermeter S. Cation Exchange in ZnSe Nanocrystals for Signal Amplification in Bioassays. *Anal. Chem.* 2011; 83: 402-408. doi: 10.1021/ac102688s
9. Ndangili PM, Jijana AM, Baker PGL, Lwuoha EI. 3-Mercaptopropionic acidcapped ZnSe quantum dot-cytochrome P450 3A4 enzyme biotransducer for 17β-estradiol. *J. Electroanal. Chem.* 2011; 653:67-74.doi:10.1016/ j.jelechem.2010.12.029
10. Ma AQ, Yu W, Huang H, Su XG. Determination of L-tyrosine based on luminescence quenching of Mn-doped ZnSe quantum dots in enzyme catalysis system. *J FLUORESC* 2011; 21:125-131. doi:10.1007/s10895-010-0696-z
11. Pol SV, Calderon-Moreno JM, Cheylan S, Gedanken A. Facile synthesis of photoluminescent ZnS and ZnSe nanopowders. *Langmuir* 2008; 24:10462-10466. doi: 10.1021/La800921a
12. Jiang Y, Meng XM, Yiu WC, Liu J, Ding, JX, Lee CS, Lee ST. Zinc Selenide nanoribbons and nanowires. *J. Phys. Chem. B.* 2004; 108: 2784-2787. doi: 10.1021/Jp035595+
13. Fanfair DD, Korgel BA. Twin-related branching of solution-grown ZnSe nanowires. *Chem. Mater.* 2007; 19: 4943-4948. doi:10.1021/Cm071440t
14. Hu ZD, Duan XF, Gao M, Chen Q, Peng LM. ZnSe nanobelts and nanowires synthesized by a closed space vapor transport technique. *J. Phys. Chem. C* . 2007; 111:2987-2991. doi: 10.1021/Jp067556e
15. Acharya S, Panda AB, Efrima S, Golan Y. Polarization properties and switchable assembly of ultranarrow ZnSe nanorods. *Adv. Mater.* 2007 ; 19: 1105-1108. doi: 10.1002/adma200602057
16. Hu JQ, Bando Y, Zhan JH, Liu ZW, Golberg D, Ringer SP. Polarization properties and switchable assembly of ultranarrow ZnSe nanorods. *Adv. Mater.* 2005; 17:975-979. doi: 10.1002/adma.200602057
17. Du J, Xu LQ, Zou GF, Chai, LL, Qian YT. A solvothermal method to novel metastable ZnSe nanoflakes. *Mater. Chem. Phys.* 2007; 103: 441-445. doi: 10.1016/ j.matchemphys.2007.02.062
18. Morales M, Vivet N, Levalois M, Bardeau JF. Optimization of ZnSe–$SiO_2$ nanostructures deposited by radio-frequency magnetron sputtering: Correlations between plasma species and thin film composition, structural and microstructural properties. *Thin Solid Films.* 2007; 515 :5314-5323. doi: 10.1016/j.tsf.2007.01.004
19. Geng BY, You JH, Zhan FM, Kong MG, Fang CH. Controllable Morphology Evolution and Photoluminescence of ZnSe Hollow Microspheres. *J. Phys. Chem. C.* 2008; 112:11301-11306. doi: 10.1021/Jp803562a
20. Wang X, Zhu JJ, Zhang YG, Jiang JG, Wei SB. One-pot synthesis and optical properties of monodisperse ZnSe colloidal microspheres. *Appl. Phys. A: Mater. Sci. Process.* 2010; 99:651-656. doi: 10.1007/s00339-010-5692-2
21. Zhang LH, Yang HQ, Xie XL, Zhang FH, Li L. Preparation and photocatalytic activity of hollow ZnSe microspheres via Ostwald ripening. *J. Alloys Compd.* 2009; 473: 65-70. doi: 10.1016/ j.jallcom.2008.06.018
22. Yao WT, Yu SH, Jiang J, Zhang L. Complex Wurtzite ZnSe Microspheres with High Hierarchy and Their Optical Properties. *Chem. Eur. J.* 2006; 12: 2066-2072. doi: 10.1002/chem.200500835
23. Schreder B, Materny A, Kiefer W, Bacher G, Forchel AL. wehr G.Resonance Raman spectroscopy on strain relaxed CdZnSe/ZnSe quantumwires. *J. Raman Spectrosc.* 2000; 31: 959-963.
24. Sarigiannis D, Peck JD, Kioseoglou G, Petrou A, Mountziaris TJ.Characterization of vapor-phase-grown ZnSe nanoparticles. *Appl. Phys. Lett.* 2002; 80: 4024-4026. doi: 10.1063/1.1481769
25. Cao HQ, Xiao YJ, Zhang SC. The synthesis and photocatalytic activity of ZnSe microspheres. *Nanotechnology* 2011; 22: 015604015612. doi: 10.1088/0957-4484/22/1/015604
26. Zhu YC, Bando Y. Preparation and photoluminescence of single-crystal zinc selenide nanowires. *Chem. Phys. Lett.* 2003; 377: 367-370. doi: 10.1016/S0009-2614(03)01197-7
27. Philipose U, Yang S, Xu T, Harry E, Ruda HE. Origin of the red luminescence band in photoluminescence spectra of ZnSe nanowires. *Appl. Phys. Lett.* 2007; 90: doi: 10.1063/1.2457190.
28. Panda AB, Glaspell G, El-Shall MS. Microwave synthesis of highly aligned ultra -narrow semiconductor rods and wires. *J. Am. Chem. Soc.* 2006; 128:2790-2791. doi: 10.1021/ja058148b
29. Sankar N, Ramachandran K. On the thermal and optical properties of ZnSe and doped ZnSe crystals grown by PVT. *J. Cryst. Growth.* 2003; 247: 157-165. doi: Pii S0022-0248(02)01982-6
30. Bukaluk A, Trzcinski A, Firszt F, Legowski S, Meczynska H. Auger depth profile analysis and photoluminescence investigations of $Zn_{1-x}Mg_xSe$ alloys. *Surface Science.* 2002; 507:175-180. doi: Pii S0039-6028(02)01208-6
31. Soderlind F, Pedersen H, Petoral RM, Kall PO, Uvdal K. Synthesis and characterisation of $Gd_2O_3$ nanocrystals functionalised by organic acids. *J. Colloid Interface Sci*. 2005; 288:140-148. doi: 10.1016j.jcis.2005.02.089
32. Liu JF, Li YD. Synthesis and self-assembly of uuminescent $Ln^{3+}$- doped $LaVO_4$ uniform nanocrystals. *Adv. Mater.* 2007; 19:1118-1122. doi: 10.1002/adma.200600336
33. Wang JL, Yang Q. One-Dimensional Angle-Shaped ZnSe Nanostructures: Synthesis and Formation Mechanism. *Cryst. Growth Des.* 2008; 8: 660-664. doi: 10.1021/Cg7008946